Polo-like kinase 1 (Plk1) overexpression enhances ionizing radiation-induced cancer formation in mice

Received for publication, August 7, 2017, and in revised form, September 5, 2017 Published, Papers in Press, September 12, 2017, DOI 10.1074/jbc.M117.810960

Zhiguo Li[‡], Jinghui Liu[‡], Jie Li[‡], Yifan Kong[‡], George Sandusky[§], Xi Rao[¶], Yunlong Liu[¶], Jun Wan[¶], and Xiaoqi Liu[‡1]

From the [‡]Department of Biochemistry, Purdue University, West Lafayette, Indiana 47907, the [§]Department of Pathology and Laboratory Medicine, Indiana University, Indianapolis, Indiana 46202, and the [¶]Department of Medical and Molecular Genetics, Indiana University School of Medicine, Indianapolis, Indiana 46202

Edited by Xiao-Fan Wang

Polo-like kinase 1 (Plk1), a serine/threonine protein kinase normally expressed in mitosis, is frequently up-regulated in multiple types of human tumors regardless of the cell cycle stage. However, the causal relationship between Plk1 up-regulation and tumorigenesis is incompletely investigated. To this end, using a conditional expression system, here we generated Plk1 transgenic mouse lines to examine the role of Plk1 in tumorigenesis. Plk1 overexpression in mouse embryonic fibroblasts prepared from the transgenic mice led to aberrant mitosis followed by aneuploidy and apoptosis. Surprisingly, Plk1 overexpression had no apparent phenotypes in the mice. Given that no malignant tumor formation was observed even after a long period of Plk1 overexpression, we reasoned that additional factors are required for tumorigenesis in Plk1-overexpressing mice. Because Plk1 can directly participate in the regulation of the DNA damage response (DDR) pathway, we challenged Plk1-overexpressing mice with ionizing radiation (IR) and found that Plk1-overexpressing mice are much more sensitive to IR than their wild-type littermates. Analysis of tumor development in the Plk1-overexpressing mice indicated a marked decrease in the time required for tumor emergence after IR. At the molecular level, Plk1 overexpression led to reduced phosphorylation of the serine/threonine kinases ATM and Chk2 and of histone H2AX after IR treatment both *in vivo* and *in vitro*. Furthermore, RNA-Seq analysis suggested that Plk1 elevation decreases the expression of several DDR genes. We conclude that Plk1 overexpression may contribute to tumor formation by both inducing chromosomal instability and suppressing the DDR pathway.

Chromosome instability and aneuploidy are hallmarks of human cancers (1). Most human cancers contain aneuploid cells, and a significant number of studies have pointed to failure in various critical mitotic events as a cause of aneuploidy in tumors (2–4). Defects in mitotic events, including centrosome maturation, microtubule-kinetochore attachment, chromosome alignment, and completion of cytokinesis, are the causes of aberrant cell division, eventually resulting in aneuploidy in daughter cells (5, 6). The regulation of proper mitotic progression that is important to genomic integrity is predominantly controlled by protein phosphorylation driven by several evolutionarily conserved serine/threonine kinases, known as mitotic kinases. The most prominent mitotic kinases include Polo-like kinase 1 (Plk1), cyclin-dependent kinase 1 (Cdk1), aurora family, and NIMA (never in mitosis A) family kinases (7).

The *Polo* gene was first cloned from *Drosophila melanogaster*, with the observation that mutations in *Polo* induced abnormal spindle poles during mitosis (8). Five mammalian homologues for *Polo*, named Plk1 to Plk15, were soon identified (9). Among them, the best characterized member of human Plk family is Plk1. It has been well-documented that Plk1 is involved in almost every step of mitosis (10). Thus, it is probably not surprising that Plk1 is overexpressed in many cancer types, including melanoma, breast, non-small cell lung, colorectal, prostate, pancreatic, ovarian, and head and neck cancers, as well as non-Hodgkin's lymphomas and acute myeloid leukemia (9, 11). More importantly, recent studies have also linked Plk1 with other cancer-associated pathways (12). For example, cross-talk between Plk1 and the p53 tumor suppressor has been described, because Plk1 negatively regulates both p53 protein stability and nuclear localization (13, 14). In another study, Plk1 elevation was shown to cause PTEN inactivation, resulting in a tumor-promoting metabolic state in prostate cancer cells (15). In line with this observation, Plk1-associated kinase activity was demonstrated to contribute to the low-dose arsenic-mediated metabolic shift from oxidative phosphorylation to glycolysis via activation of the PI3K/AKT/mTOR pathway (16). In addition, elevation of Plk1 leads to acquisition of resistance to various therapies, including radiotherapy (17), taxol (18), metformin (19), gemcitabine (20, 21), and androgen signaling inhibitors (22). All these studies strongly suggest that Plk1 likely plays a critical role during carcinogenesis.

Inhibition of cell proliferation and induction of apoptosis are two basic principles of anticancer therapy. Antimitotic therapy is a standard of care for many cancer types. Overexpression of Plk1, observed in a broad spectrum of cancers, has often been correlated with disease stage, histologic grade, poor prognosis, metastatic potential, and survival (9). The key role of Plk1 in oncogenic events gave impetus to the development of potent

This work was supported by National Institutes of Health Grants R01 CA157429 (to X. L.), R01 CA192894 (to X. L.), R01 CA196835 (to X. L.), R01 CA196634 (to X. L.), and P30 CA023168 (to the Purdue University Center for Cancer Research). The authors declare that they have no conflicts of interest with the contents of this article. The content is solely the responsibility of the authors and does not necessarily represent the official views of the National Institutes of Health.

This article contains supplemental Fig. S1.

[1] To whom correspondence should be addressed: Dept. of Biochemistry, Purdue University, 175 S. University St., West Lafayette, IN 47907. Tel.: 765-496-3764; Fax: 765-494-7897; E-mail: liu8@purdue.edu.

and specific small molecule Plk1 inhibitors (10). Consequently, several Plk1 inhibitors have been developed, with some agents showing encouraging results in various cancer cell lines and xenograft models of human cancer (23, 24). Preclinical studies have demonstrated a particular sensitivity to Plk1 inhibition in human cancer cells harboring specific genetic abnormalities, including mutations in *p53*, *Ras*, and *PTEN* (10). In contrast to marked antitumor activity in leukemia, overall antitumor activity of Plk1 inhibitors in patients with solid tumor has been modest in trials (23). Thus, there is a critical need for understanding the physiological functions of Plk1 *in vivo*. Lack of Plk1 transgenic mice is one major hurdle to achieve that.

Herein, we generated a transgenic mouse model to investigate the involvement of Plk1 in tumorigenesis. Using a Cre-loxP system, we achieved the conditional expression of Plk1. Elevated Plk1 expression resulted in mitotic failure, leading to apoptosis and aneuploidy in mouse embryonic fibroblasts (MEFs).[2] In addition, Plk1 overexpression caused a defective DNA damage response (DDR) pathway. Our findings indicated that this mouse model is a useful system to study the physiological roles of Plk1 in cancer etiology and therapeutics.

Results

Strategy and design for the conditional Plk1 transgenic mouse

Considering that overexpression of Plk1 induces abnormalities in cell division *in vitro*, we selected a conditional transgenic system to prevent the possible embryonic lethality of founder animals (Fig. 1*A*). The configuration of this transgenic cassette was chosen so that Plk1 would be overexpressed in the transgenic mice after expression of Cre recombinase. To prevent the chromosomal positional effects associated with the random nature of transgenic integration, we inserted the cassette into the well-characterized euchromatic locus Rosa26 (Fig. 1*A*). The standard transfection procedures using this exchange vector were followed by the recombinase-mediated integration, which resulted in more than 90% positive embryonic stem (ES) cell clones (Fig. 1, *B–H*). Plk1-KI mice were subsequently obtained from the recombinant ES cells.

Establishment and characterization of transgenic mouse founders for Plk1 expression

We successfully obtained four conditional transgenic founders by pronuclear injection to mouse embryos. Female conditional Plk1-KI mice were mated with male CMV-Cre transgenic mice that have a wide tissue distribution for expression of Cre recombinase (25). Expression of Plk1 in CMV-Cre/Plk1-KI double transgenic mice was detected in several organs with quantitative RT-PCR (qRT-PCR) (Fig. 2*A*), immunoblotting (IB) analysis (Fig. 2*B*), and immunohistochemistry (IHC) staining (Fig. 2*C*). Increase of Plk1 expression was also confirmed in CMV-Cre/Plk1-KI MEFs (Fig. 2*D*). To further validate the Plk1 overexpression system, Plk1-KI mice were crossed with Myod-Cre mice, which express Cre in a muscle-specific manner. As indicated, Plk1 expression was detected only in muscle in Myod-Cre/Plk1-KI mice (Fig. 2, *E* and *F*). These data indicate that the Plk1 conditional transgenic system works properly *in vivo*.

Elevated Plk1 expression leads to mitotic abnormalities and apoptosis in late-passage mouse embryonic fibroblasts

Considering that Plk1 has multiple functions during the cell cycle, we next examined the effects of Plk1 overexpression on the proliferation and cell-cycle progression of MEFs. Overexpression of Plk1 was confirmed in MEFs isolated from two different CMV-Cre/Plk1-KI mouse lines (supplemental Fig. S1*A*). Surprisingly, massive Plk1 overexpression had no apparent impact on the proliferative activity of early-passage MEF lines compared with control MEFs (supplemental Fig. S1*B*). Furthermore, we assessed the potential correlation between Plk1 overexpression and cell cycle distribution. Despite much higher levels of the Plk1 expression in CMV-Cre/Plk1-KI lines, FACS analyses showed no apparent increase in G_2/M populations compared with control MEF cells (supplemental Fig. S1iC). Given that MEFs undergo abnormal mitosis and senescence at late passages, we tested whether Plk1 overexpression affects this process. Interestingly, induction of Plk1 overexpression resulted in significantly increased abnormal mitotic figures in late-passage MEFs (Fig. 3*A*). Staining by propidium iodide showed various mitotic defects, including chromosome misalignment, chromosome missegregation, and chromosome bridges, observed at higher rates in late-passage Plk1-overexpressing MEFs (Fig. 3*A*). To further assess the chromosome instability induced by Plk1 overexpression, we analyzed chromosome spreads generated from serial passages of MEFs according to the 3T3 protocol (Fig. 3*B*). The total number of chromosomes in each cell was determined, and cells were scored as diploid (2n = 40) or aneuploid. Primary control MEFs, under normal culture conditions, spontaneously become aneuploidy. However, we found that Plk1-overexpressing MEFs were significantly more aneuploidy than control MEFs at later passages (Fig. 3*B*). Examination of the absolute number of chromosomes per cell revealed a highly significant increase in the frequency of di- and multinucleated cells compared with control MEFs.

The proliferation of control and Plk1-overexpressing MEFs at later passages was investigated using MTT assay. Control MEF cells was observed to proliferate significantly faster than the Plk1-KI cells at passage 5 (Fig. 3*C*). To determine whether the growth arrest in the Plk1-KI MEFs was associated with cell cycle defects, DNA content was analyzed. We found that Plk1-KI cells at passage 5 caused a significant increase in the cell number of cells in G_2/M phase, concomitant with a significant decrease in the percentage of cells in G_0/G_1 phase (Fig. 3*D*). Furthermore, MEFs with overexpression of Plk1 exhibited a substantial increase in the sub-G_1 population, suggesting that a large number of cells at G_2/M phase underwent cell death (Fig. 3*D*). Using senescence-associated β-galactosidase assay, we found that Plk1-overexpressing MEFs displayed an increased senescence phenotype (Fig. 3*E*).

[2] The abbreviations used are: MEF, mouse embryonic fibroblast; DDR, DNA damage response; IR, ionizing radiation; ES, embryonic stem; qRT-PCR, quantitative RT-PCR; IB, immunoblotting; IHC, immunohistochemistry; GTT, glucose tolerance test; FC, fold change; DEG, differentially expressed gene; KI, knock-in; RMCE, recombination-mediated cassette exchange; H&E, hematoxylin and eosin.

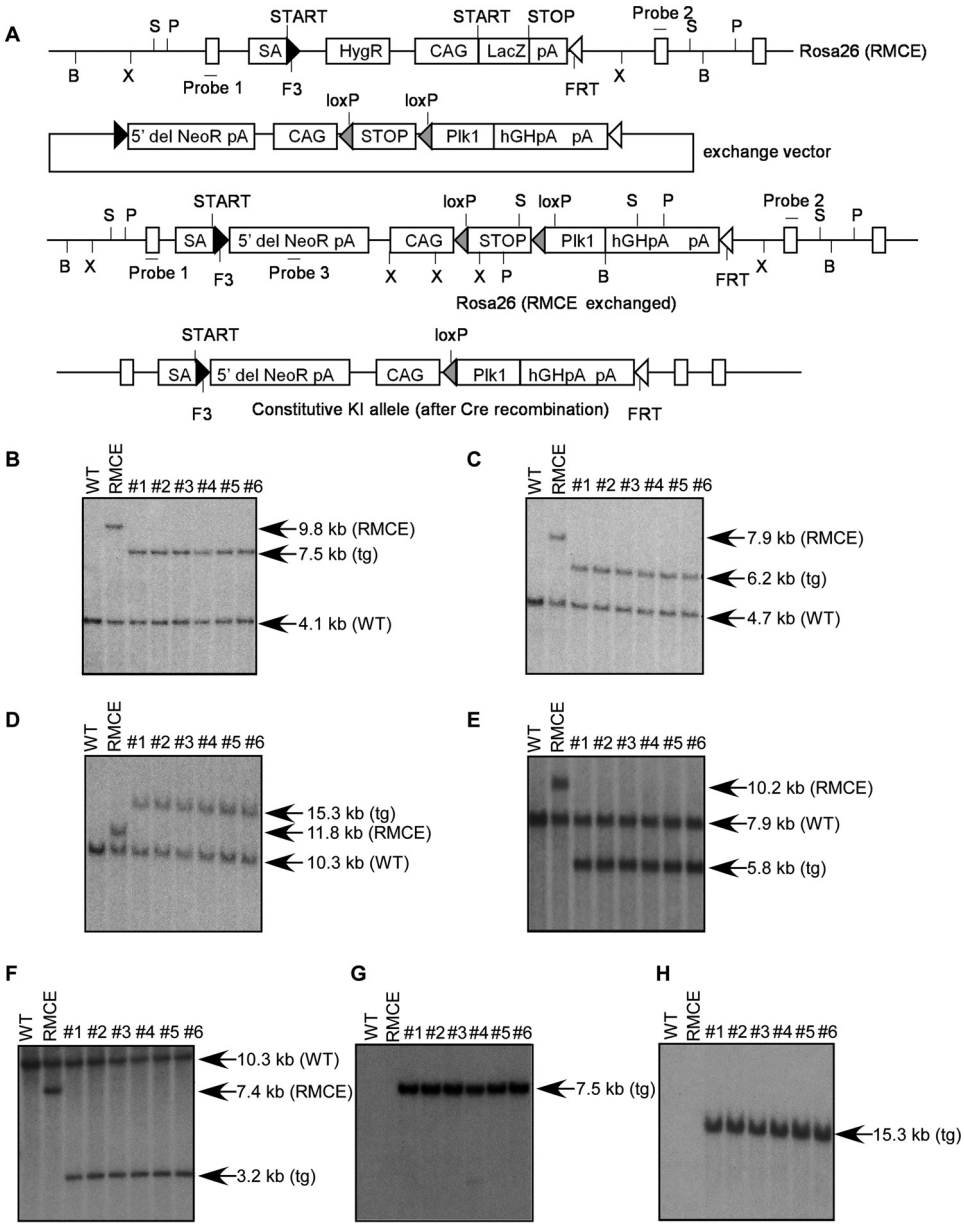

Figure 1. Generation of Plk1-KI mice. *A*, recombination-mediated cassette exchange (RMCE) technology was used to generate Plk1-KI mice. The Rosa26 targeting vector, which comprises of the HygR and cytomegalovirus-enhancer/β-actin (CAG)-LacZ, was inserted into the Rosa26 locus using recombination cassette exchange in ES cells. The F3/FRT sites were oriented in opposite directions. The modified locus equipped with RMCE docking sites is called Rosa26 (RMCE). The exchange vector carries the following elements: a CAG promoter sequence, a loxP-flanked transcription termination cassette (STOP) containing a combination of polyadenylation signals (human growth hormone and synthetic polyadenylation signals), the mouse Plk1 ORF together with a Kozak sequence, the human growth hormone polyadenylation signal and an additional polyadenylation signal, the F3/FRT pair, and a truncated neoR (neomycin resistance) gene for positive selection. A poly(A) signal is included to prevent the expression of truncated neoR and Plk1 gene at random integration sites. After the exchange vector was transfected into the C57Bl/6 ES cell line equipped with RMCE docking sites in the Rosa26 locus, the resulting clones, mediated by FLP recombination, were isolated using positive NeoR selection (Rosa26; RMCE exchanged). ES cells were injected into diploid blastocysts, and chimera were generated. Finally, cross-breeding of chimeric with C57BL/6 mice to produce mice heterozygous for the conditional targeted Plk1 transgene. The presence of the transcription termination cassette prevents expression of Plk1 protein form the conditional KI allele. Plk1 will be expressed from the CAG promoter after Cre-mediated deletion of the transcription termination cassette. The constitutive Plk1-KI allele can be obtained after Cre-mediated recombination. *S*, SspI; *B*, BmtI; *X*, XbaI; *P*, PacI. *B–H*, Southern blotting analyses of genomic DNA from ES cells. *RMCE*, Rosa26 (RMCE); *#1–#6*, six transgenic (*tg*) ES clones. *B*, genomic DNA was digested with SspI and analyzed using probe 1. The sizes of WT, Rosa26 (RMCE), and Rosa26 (RMCE exchanged) were 4.1, 9.8, and 7.5 kb, respectively. *C*, genomic DNA was digested with XbaI and analyzed using probe 1. The sizes of WT, Rosa26 (RMCE), and Rosa26 (RMCE exchanged) were 4.7, 7.9, and 6.2 kb, respectively. *D*, genomic DNA was digested with Bmt1 and analyzed using probe 1. The sizes of WT, Rosa26 (RMCE), and Rosa26 (RMCE exchanged) were 10.3, 11.8, and 15.3 kb, respectively. *E*, genomic DNA was digested with PacI and analyzed using probe 2. The sizes of WT, Rosa26 (RMCE), and Rosa26 (RMCE exchanged) were 7.9, 10.2, and 5.8 kb, respectively. *F*, genomic DNA was digested with BmtI and analyzed using probe 2. The sizes of WT, Rosa26 (RMCE), and Rosa26 (RMCE exchanged) were 10.3, 7.4, and 3.2 kb, respectively. *G*, genomic DNA was digested with SspI and analyzed using probe 3. The size of Rosa26 (RMCE exchanged) was 7.5 kb. In transgenic clones #1–#6, integration of neomycin-resistant gene was detectable, whereas, as expected, WT and Rosa26 (RMCE) showed no signal for the exchange vector. *H*, genomic DNA was digested with BmtI and analyzed using probe 3. The size of Rosa26 (RMCE exchanged) was 15.3 kb. Integration of neomycin-resistant gene was observed in all six transgenic clones, but not in WT and Rosa26 (RMCE).

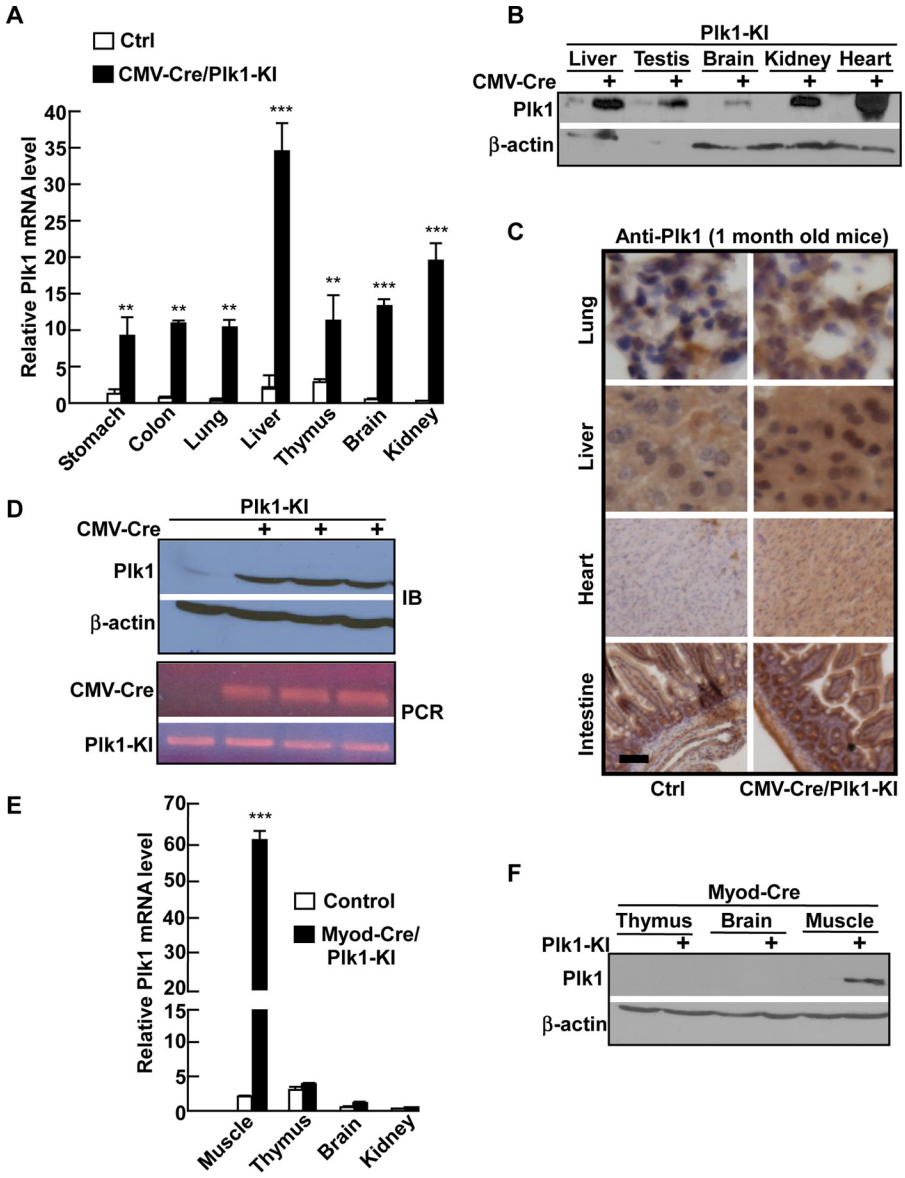

Figure 2. Plk1 detection in the tissues of double transgenic mice (CMV-Cre/Plk1-KI). *A*, relative Plk1 mRNA levels in the tissues of CMV-Cre/Plk1-KI animals were compared with the levels in Plk1-KI but without Cre expression (Control, *Ctrl*) animals (mean ± S.D., $n = 3$ for each tissue). *B*, total cellular protein was prepared from the indicated tissues of adult CMV-Cre/Plk1-KI or control mice and subjected to IB. *C*, animals were sacrificed at the age of 1 month, followed by anti-Plk1 IHC staining of indicated tissues. Sections representing the organs of control (Plk1-KI only) and CMV-Cre/Plk1-KI mice. *Bar*, 200 μm. *D*, *top panel*, whole cell extracts from MEFs isolated from CMV-Cre/Plk1-KI and control animals were subjected to IB. *Bottom panel*, PCR of mouse genomic DNA (tail clips) are presented. *E*, relative Plk1 mRNA levels in the tissues of Myod-Cre/Plk1-KI animals were compared with the levels in control animals (mean ± S.D., $n = 3$ for each tissue). *F*, total cellular protein was prepared from the indicated tissues of Myod-Cre/Plk1-KI and control mice. **, $p < 0.05$; ***, $p < 0.01$.

Phenotypic analysis of Plk1-KI mice

The CMV-Cre/Plk1-KI double transgenic mice displayed no apparent developmental abnormalities during mouse development. They grew and gained weight normally during the first 9 months of their life. However, by 18 months of age CMV-Cre/Plk1-KI mice exhibited slightly reduced weight compared with WT littermates (Fig. 4*A*). Litter sizes were similar for CMV-Cre/Plk1-KI and WT mice, ranging from 7 to 9 pups per litter. The pups were born healthy and developed normally at a normal growth rate, maturing at the age of 3–4 weeks. Further, we did not observe any obvious behavioral difference between CMV-Cre/Plk1-KI and WT animals. However, a minor reduced survival rate in Plk1-KI mice was observed, when the mice were monitored up to 25 months of age (Fig. 4*B*). The complete morphological analyses did not reveal significant histological differences between the organs of CMV-Cre/Plk1-KI mice and WT animals at the ages of both 1 and 11 months (Fig. 4, *C* and *D*). To determine the consequences of Plk1 overexpression on whole-body energy balance, we performed indirect calorimetry analyses. On a chow diet, CMV-Cre/Plk1-KI mice showed a slightly higher energy expenditure than control mice, as indicated by both slightly increased O_2 consumption (Fig. 4*E*) and slightly increased CO_2 production (Fig. 4*F*). Considering that Plk1 is critical for energy metabolism in cultured cells (16), we examined the glucose uptake in a glucose tolerance test (GTT). Glucose uptake from CMV-Cre/Plk1-KI mice was slightly increased in comparison to WT littermates (Fig. 4*G*). Given that Plk1 is essential for many mitotic events, we exam-

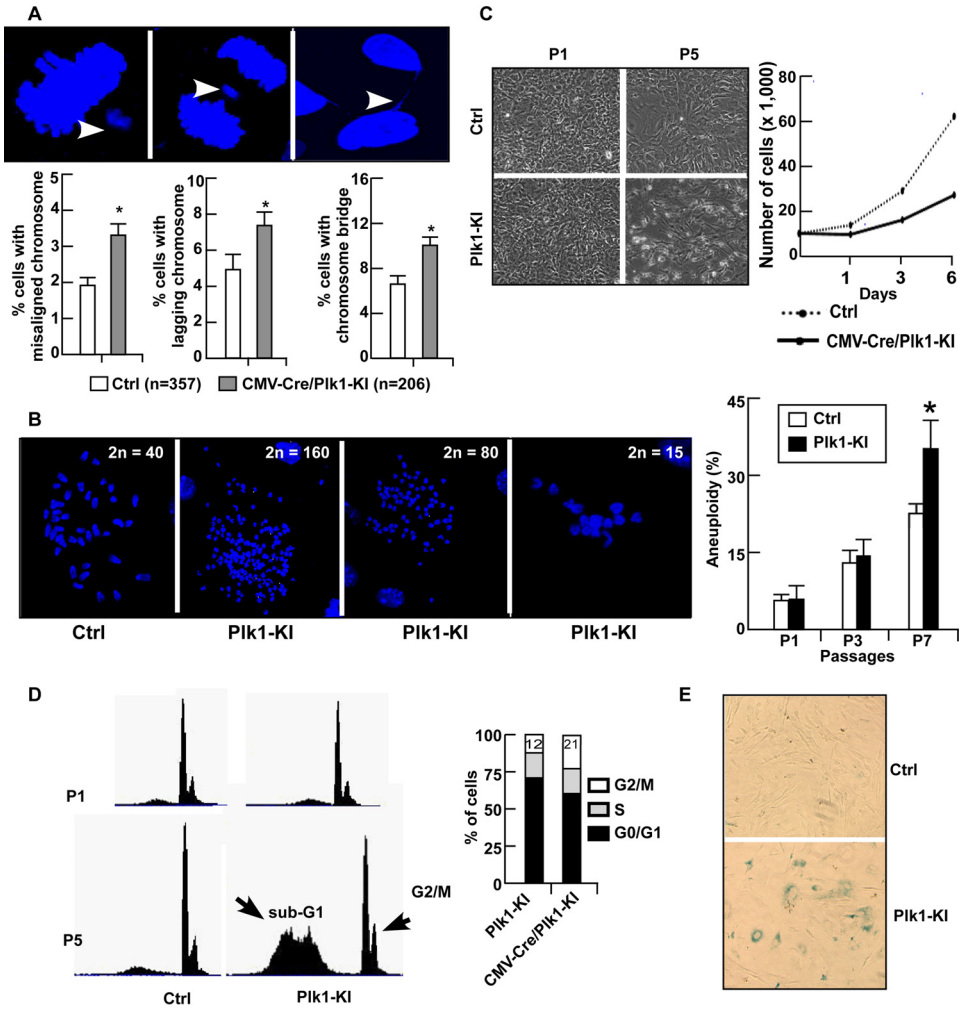

Figure 3. Plk1 overexpression causes aneuploidy and apoptosis in MEFs. *A*, Plk1 overexpression causes various chromosome segregation errors. *Upper panel*, the *left image* shows a metaphase cell with misaligned chromosomes, whereas the *middle image* is an example of anaphase cell with lagging chromosomes. The *right image* shows cells with a chromosome bridge. *Arrows* indicate various chromosome segregation defects described above. *Bottom panel*, histograms showing the percentages of cells with various chromosome segregation errors in Plk1-overexpressing cells. *B*, representative chromosome spreading of Plk1-overexpressing MEFs, with WT MEFs spreading with 40 chromosomes (*left panel*). The percentages of aneuploid cells were calculated from metaphase spreads of control (*Ctrl*) and Plk1-overexpressing MEFs at different passages cultured according to the 3T3 protocol ($n = 3$ experiments with 50 spreads each) (*right panel*). *C*, analysis of proliferation capacity of control and Plk1-overexpressing MEFs. Cells at passage 5 were seeded at a density of 1×10^4 cells/well and monitored at indicated times by cell counting. *D*, flow cytometric analysis of cell-cycle distribution of late-passage of Plk1-overexpressing MEFs. The cells were collected, stained with propidium iodide, and subjected to DNA content analysis with flow cytometry. Histograms on the *right* show the average percentages of cells in $G_{0/1}$, S, and G_2/M phases. *E*, senescence assay for control and Plk1-overexpressing MEFs. The cells were fixed and subjected to senescence associated β-galactosidase assay.

ined the proliferative activity in CMV-Cre/Plk1-KI mice by staining Ki67 of various tissues. The proliferation index was moderately increased only in the liver (see Fig. 6*A*).

Plk1-KI mice and MEFs are hypersensitive to DNA damage

Because no malignant tumor formation was detected in the Plk1-overexpressing mice after a long latency, we then challenged Plk1-overexpressing mice with carcinogens to see whether Plk1 overexpression affects carcinogenesis under stimulation condition. Mounting evidence suggests that Plk1 directly participates in the regulation of DNA double-strand break repair (26, 27). We therefore explored whether Plk1 overexpression affects cellular response to DNA damage *in vivo*. Cohorts of CMV-Cre/Plk1-KI and WT mice were irradiated with 10 Gy of ionizing radiation (IR) and closely monitored for radiation toxicity. Although ~60% of WT littermates ($n = 14$) survived beyond 50 days, over 80% of CMV-Cre/Plk1-KI animals ($n = 15$) died within 50 days (Fig. 5*A*), indicating that CMV-Cre/Plk1-KI mice were more sensitive to IR) than WT littermates. To confirm this observation, we plated MEFs (WT or CMV-Cre/Plk1-KI) at clonal density and exposed to increasing doses of IR, followed by colony formation assay. In agreement with the *in vivo* results, the viability of CMV-Cre/Plk1-KI MEFs after IR was significantly impaired compared with WT MEFs, indicating that Plk1-overexpressing MEFs are more sensitive to DNA damage induced by IR (Fig. 5*B*). In a separate experiment, CMV-Cre/Plk1-KI and WT mice at the age of 10 weeks were exposed to a single dose of 5 Gy whole body γ-ray irradiation and monitored for additional 4 months. CMV-Cre/Plk1-KI, but not WT, mice showed severe dermatitis, scratching bloody areas in head, neck, and ears (Fig. 5*C*). Although none of WT mice had tumors after 4 months, 10.3% of CMV-Cre/Plk1-KI developed life-threatening spleen lymphomas, a difference that was statistically significant ($p = 0.0386$; Fig. 5*D*,

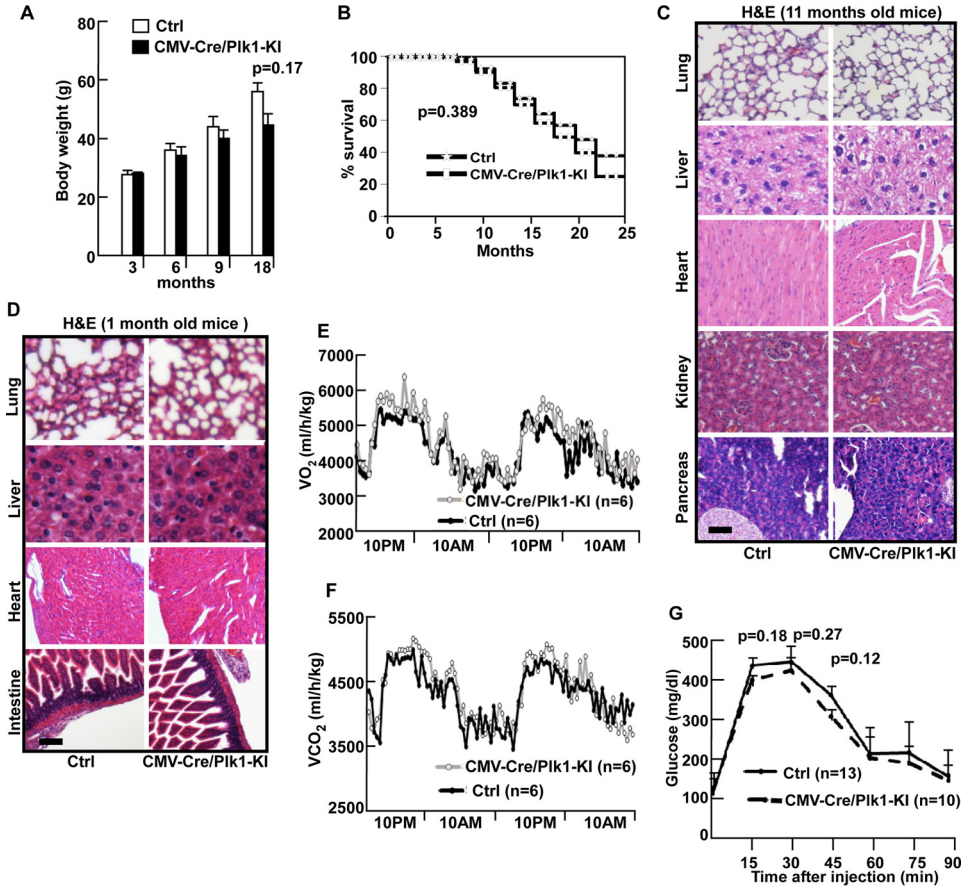

Figure 4. Phenotypic analyses of Plk1-KI mice. *A*, the body weights of control (*Ctrl*) and CMV-Cre/Plk1-KI mice at different ages. *Open* and *shaded bars* correspond to control and CMV-Cre/Plk1-KI mice, respectively. The values are means ± the standard errors of means. A Student's *t* test was used to calculate *p* values (n = 7–11 mice per group). *B*, survival of control *versus* Plk1-KI mice (n = 15–17 mice/group) over a period of 25 months. *C* and *D*, animals were sacrificed at the ages of 1 or 11 months, followed by H&E staining of indicated tissues. Sections representing the organs of control and CMV-Cre/Plk1-KI mice are shown. *Bars*, 200 μm. *E* and *F*, Plk1 overexpression increases energy expenditure in mice. Male mice fed with regular chow were subjected to indirect calorimetry. Oxygen consumption (*E*) and carbon dioxide release (*F*) were determined in control and CMV-Cre/Plk1-KI mice in metabolic chambers (n = 6/group). *G*, Plk1 overexpression results in increased glucose uptake in a GTT. 2-month-old male mice were starved for 16 h and injected with glucose, followed by measurement of blood glucose levels at the indicated times.

bottom panel). Upon IR, CMV-Cre/Plk1-KI mice showed apparent splenic enlargement and disruption of normal splenic architecture, forming diffused lymphoma (Fig. 5*D*, *top panel*). Increased radiation sensitivity is one of the hallmarks of defective DDR. The results described above suggested that Plk1 elevation leads to inhibition of DDR. To directly test this hypothesis, we analyzed DDR of mice. Spleens were prepared from three different mice that were exposed to IR and subjected to IB to follow the DDR pathway. IR led to activation of DDR, indicated by elevated phosphorylation of ATM, Chk2, and H2AX in WT, but not in CMV-Cre/Plk1-KI mice (Fig. 5*E*). Finally, IR also led to activation of the ATM/Chk2 pathway in WT but not in CMV-Cre/Plk1-KI MEFs (Fig. 5*F*).

Overexpression of Plk1 leads to increased proliferation and hypersensitivity to DNA damage in liver

Because liver is the only tissue that showed increased proliferation upon Plk1 overexpression in the absence of IR (Fig. 6*A*), we further analyzed liver-associated phenotypes after IR. A 4-fold increase in liver tumors in CMV-Cre/Plk1-KI *versus* normal littermates was observed (p = 0.0472; Fig. 5*D*, *bottom panel*). Upon IR, the livers of CMV-Cre/Plk1-KI mice were apparently enlarged and carrying small tumors compared with WT controls (Fig. 6*B*). IR of WT mice led to multifocal lymphoid hyperplasia, seen in a perivascular location (Fig. 6*C*, *top panel*). For IR-treated CMV-Cre/Plk1-KI mice, we observed multiple lymphocytic overgrowth in the parenchyma and mitotic figures, suggesting the formation of mild lymphoma (Fig. 6*C*, *middle panel*) or severe lymphoma (Fig. 6*C*, *bottom panel*). To determine whether lymphoma in IR-treated CMV-Cre/Plk1-KI mice is of T-cell or B-cell origin, we stained a T cell marker with CD3. Approximately 80–90% of the neoplastic round cells demonstrated moderate to strong positive staining with CD3 antibody, indicative of T lymphocyte origin (Fig. 6*D*). Further, Ki67 IHC staining was performed to the same samples. Ki67 signal was virtually undetectable in WT samples but significantly increased in lymphoma areas of CMV-Cre/Plk1-KI mice (Fig. 6*E*). Finally, we also observed apparent diffuse and sever fatty change in the parenchyma of liver of one CMV-Cre/Plk1-KI mouse (Fig. 6*F*).

To understand how Plk1 overexpression accelerates IR-induced cancer formation, we performed an RNA-Seq analysis of MEFs under different conditions (± Plk1-KI ± IR irradiation). Expression levels of 648 genes were affected upon Plk1 overex-

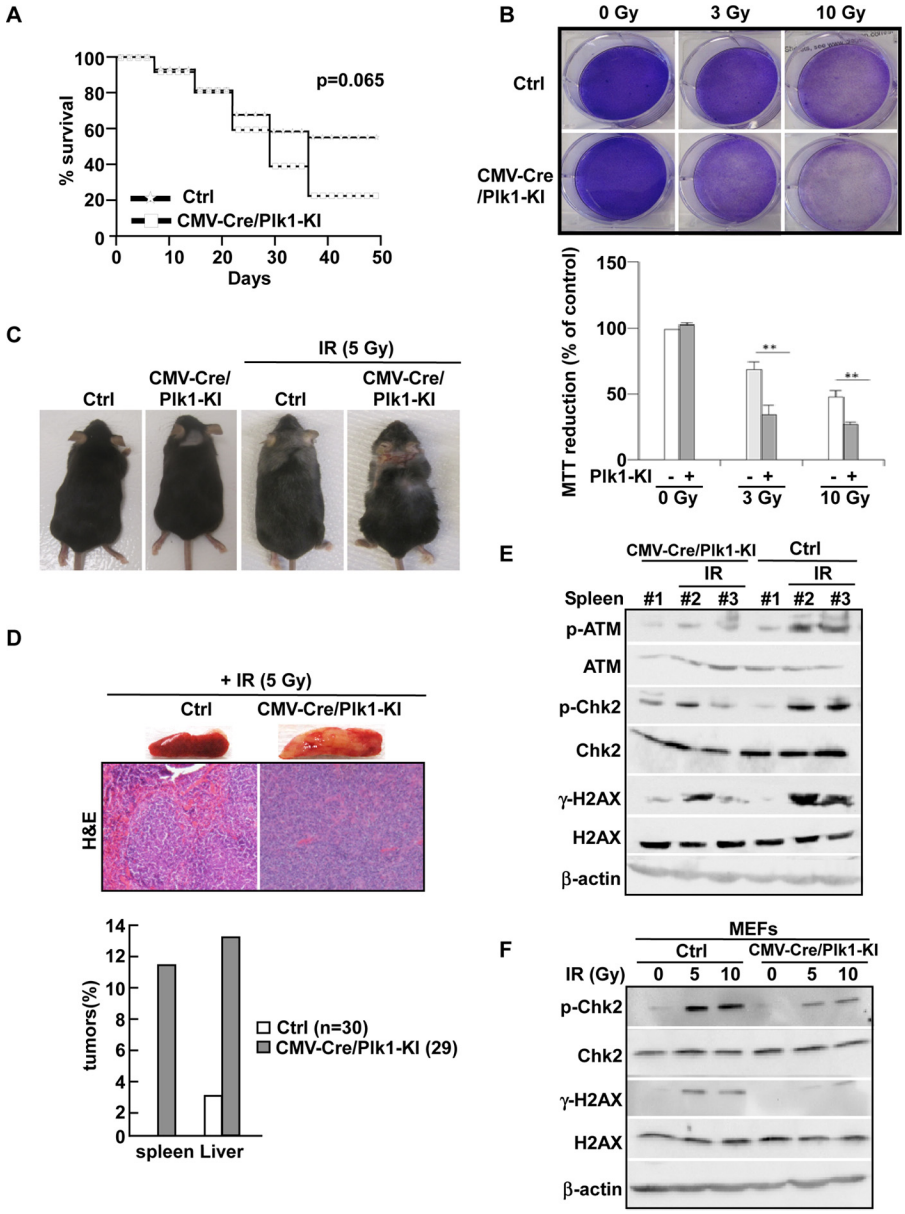

Figure 5. Plk1-KI mice are hypersensitive to IR. *A*, survival plot to compare survival of CMV-Cre/Plk1-KI and control (*Ctrl*) mice after whole body IR with 10 Gy. *B*, MEFs from control and CMV-Cre/Plk1-KI mice were plated at clonal density and subjected to increasing doses of IR. The number of colonies appearing after 10 days on the irradiated plates indicate the reduced viability of Plk1-overexpressing MEFs upon IR exposure. To quantify the number of cells remaining on the plates after IR, samples were stained with MTT and lysed, and absorbance was measured with a standard plate reader. The values reported are means ± S.D. of three independent experiments (*bottom panel*). **, $p < 0.01$. *C*, mice at the age of 10 weeks were subjected to 5 Gy whole body irradiation and imaged after 4 months. *D*, *top panel*, representative H&E-stained sections of spleen of CMV-Cre/Plk1-KI and control mice after 5 Gy whole body IR as in *C*. *Bottom panel*, CMV-Cre/Plk1-KI animals develop elevated levels of spleen and liver tumors after exposure to IR. *E*, mice (CMV-Cre/Plk1-KI or control) were either left untreated or exposed to 12.5 Gy of IR and sacrificed at 4 h post-irradiation. Spleen samples were analyzed by IB with the indicated antibodies. *F*, MEFs of CMV-Cre/Plk1-KI or control animals were irradiated at the indicated doses, followed by IB with indicated antibodies.

pression, whereas most of the affected genes were down-regulated. In the presence of IR irradiation, Plk1 overexpression led to modulation of 227 genes (Fig. 7, *A* and *B*). This observation is expected because it has been documented that Plk1 is a target of DNA damage. Plk1 KI affects the expression of 97 genes in both the presence and the absence of IR irradiation. Detailed description and analysis of RNA-Seq data will be reported separately. Herein, we only focus on genes related to DNA damage repair pathways. As indicated in Fig. 7*C*, Plk1 overexpression clearly affects the expression of a series of DNA damage repair genes. In addition, RT-PCR was performed to confirm this observation (Fig. 7*D*). Thus, deregulation of DNA damage repair pathways upon Plk1 overexpression is the likely reason to explain the enhanced IR-induced cancer formation.

Discussion

Mitotic kinases are critical regulators of cell cycle progression, and the timing of expression and activities of those kinases are tightly regulated during the cell cycle. Plk1 is associated with mitotic spindle poles and centromere/kinetochore regions and the expression and activity of Plk1 peak during late G_2 to M phase (9, 10). Although the majority of studies highlights the

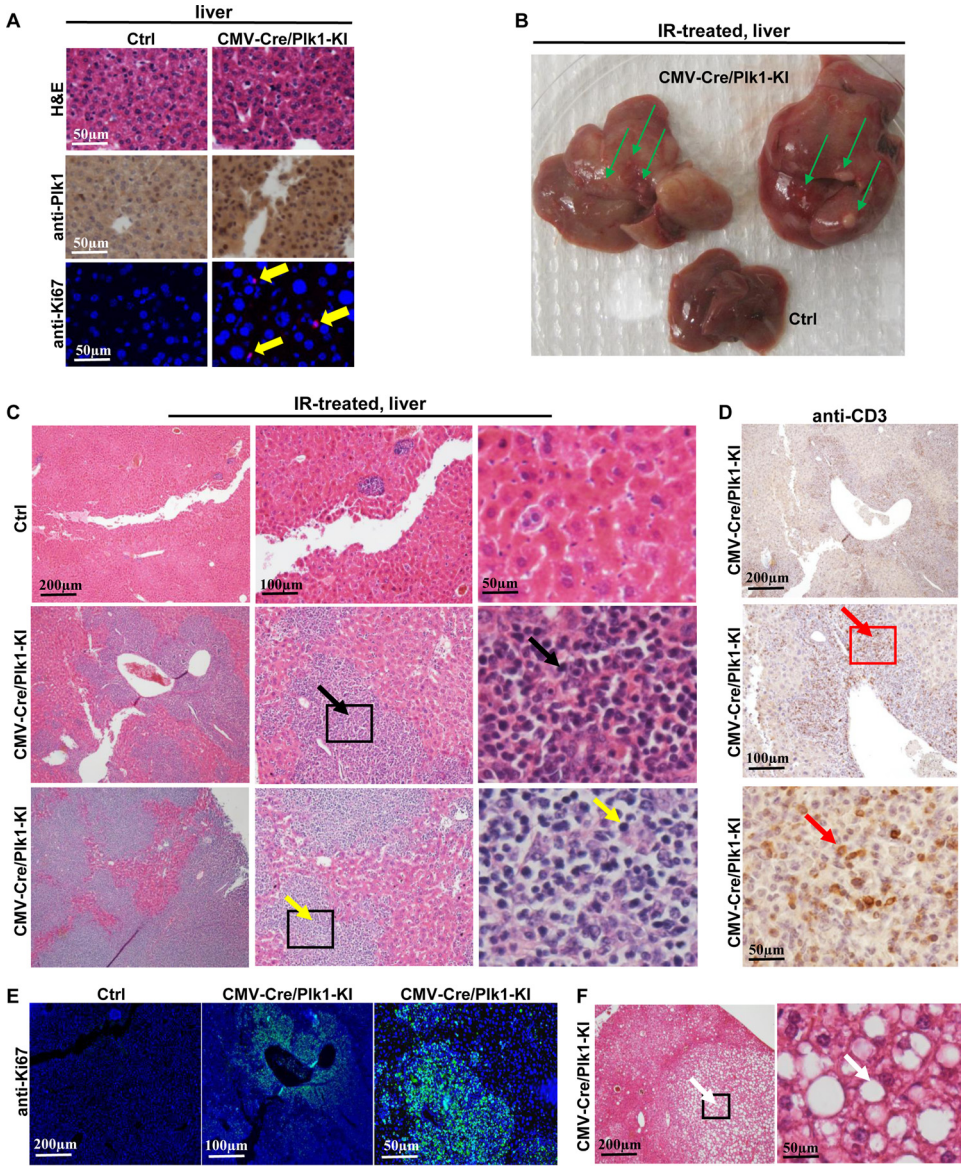

Figure 6. Increased incidence of lymphoma or severe fatty change in the Plk1-KI mice after radiation. *A*, overexpression of Plk1 in the liver of the CMV-Cre/Plk1-KI mice. *B–F*, mice (control (*Ctrl*) or CMV-Cre/Plk1-KI) were euthanized 40 days after 5 Gy whole body IR. *B*, representative images of liver at the end of study with *green arrows* indicating the tumors on the surface. *C*, representative images of H&E staining of liver sections from mice with *black* and *yellow arrows* indicating the mild and severe lymphomas, respectively. *D*, IHC staining for T cell marker CD3 with the sections in C with *red arrows* indicating the positive CD3 signals. *E*, IF staining for the Ki67 with sections in *C*. *F*, representative images of H&E staining of liver section from one of the Plk1-KI mice with *white arrows* indicating severe fatty change.

essential role of Plk1 for mitosis, overexpression of Plk1 is often observed in interphase of many cancer cell lines and tumor samples. In addition to these pathological observations, evidence that Plk1 overexpression in NIH3T3 cells induces tumor formation in nude mice suggests that dysregulation of Plk1 expression is a potential cause of sporadic malignant tumors (28). These observations have prompted research into the potential therapeutic application of Plk1 inhibition in cancer. Mitotic catastrophe and tumor growth inhibition have been observed in preclinical studies using Plk1 inhibitors or siRNAs (12, 29). However, with all the evidence pointing to Plk1 as a worthwhile cancer target, it should be noted that the molecular evidence of Plk1 being a *bona fide* oncogene is still lacking. Accordingly, we have established a Plk1 transgenic mouse line to achieve overexpression of Plk1 with a new conditional transgenic system. In this system, the expression of Plk1 is regulated by the recombination with the transgene mediated with Cre protein and its target sequences.

Previous cellular studies indicate that sustained overexpression of Plk1 increases the oncogenic potential of cultured cells (28). Herein, we have taken advantage of a conditional expression model to modulate the expression of Plk1. Our data based on MEFs confirmed the effect of Plk1 overexpression on the generation of misaligned chromosome and aneuploidy. We have also observed that Plk1 overexpression induces apoptosis in cultured MEFs at later passages. Several studies have indicated that expression of activated oncogenes, such as Aurora-A or Myc, generally induces apoptotic cell death in MEFs. Further, apoptotic cell death induced by Aurora-A or Myc has been demonstrated to be p53-dependent (30–32). Because studies

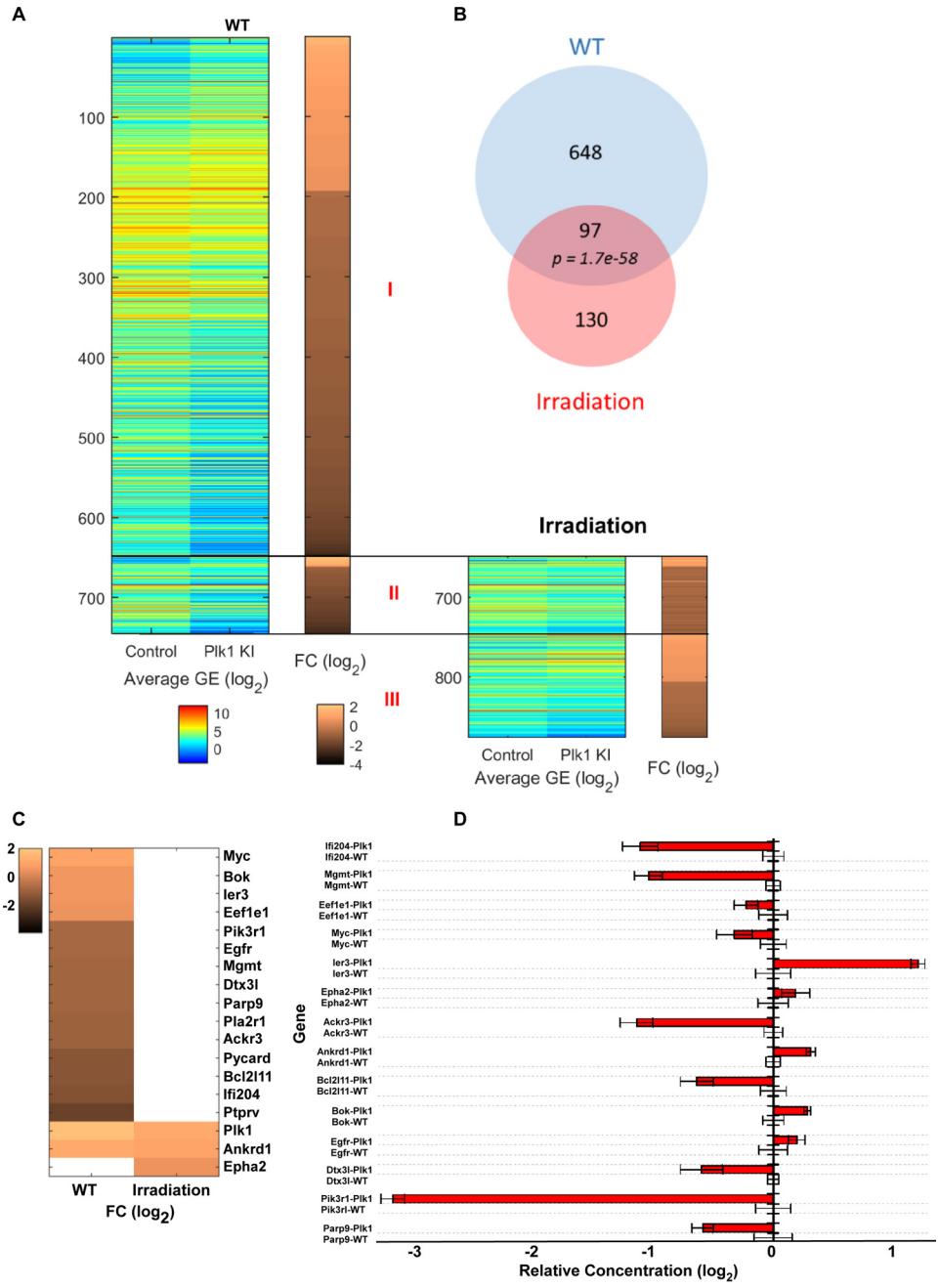

Figure 7. Plk1 overexpression inhibits expression of DNA damage repair genes. *A*, heat map of average gene expression and FC of total 875 DEGs between Plk1 KI and control for WT and irradiation, respectively. The DEGs were sorted by the FCs from the highest to the lowest and separated into three groups: *group I*, 648 DEGs for WT only; *group II*, 97 DEGs for both WT and irradiation; and *group III*, 130 DEGs for irradiation only. *B*, Venn diagram of numbers of DEGs for WT and for irradiation. It shows statistically significant overlap between two groups of DEGs ($p = 1.7e\text{-}58$). *C*, FCs of DEGs associated with DNA damage/repair based on gene ontology association. *D*, RT-PCR of DNA damage/repair genes of MEFs (WT *versus* Plk1-KI).

have also revealed a connection between Plk1 and p53, it is possible that p53 might be involved in apoptosis of MEFs with deregulated Plk1. It was shown that Aurora-A overexpression in mammary epithelial cells results in increased apoptosis, with a low frequency of tumor formation that is accelerated in a p53-null background (32). It should be interesting to test whether Plk1 overexpression accelerates tumor formation in a p53-null background.

To our surprise, Plk1 overexpression alone is not enough to drive cancer initiation, indicating that additional genetic modifications are required for tumor formation. Of note, inducible Plk1 knockdown mice described previously did not show any significant phenotype either (33). Increasing evidence suggests that Plk1 is directly involved in overall DNA damage response, including DNA damage checkpoint activation, checkpoint maintenance, damage recovery, and DNA repair (34). Accordingly, we challenged Plk1-overexpressing mice with IR to ask whether Plk1 overexpression affects DDR pathway. Indeed, Plk1 overexpression clearly showed increased radiation sensitivity and accelerated IR-induced carcinogenesis in mice. Based on our observation, we postulate that Plk1 is a critical regulator of IR-induced carcinogenesis, likely because of premature

checkpoint termination and reduced DNA repair in Plk1-KI mice.

We understand that most of previous studies suggested that Plk1 plays an important role in turning off the later stages of DDR. Interestingly, we recently found that Plk1 also phosphorylates key factors upstream of ATM/ATR and regulates their DDR-related functions in human cells. Specifically, Plk1 directly phosphorylates Mre11, a component of the Mre11–Rad50–Nbs1 complex, at serine 649 during DDR. Phosphorylation of Mre11 inhibited loading of the Mre11–Rad50–Nbs1 complex to damaged DNA, leading to checkpoint termination and inhibition of DNA repair (35). This is one likely mechanism to explain why Plk1 KI mice are hypersensitive to ionizing radiation, because Plk1-overexpressed cells will continue to cycle even in the presence of DNA damage, eventually resulting in a much higher chance for tumorigenesis. In addition, Plk1-KI leads to inactivation of p53 and PTEN, two most important tumor suppressors. This statement has been supported by many of our previous publications. For example, we once showed that Plk1 depletion leads to p53 stabilization (36). Mechanistically, we later showed that Plk1 phosphorylation of GTSE1 and Topors, two negative regulators of p53, results in p53 inactivation (13, 14). Directly related to Plk1-KI mouse work, we recently showed that Plk1 KI causes p53 inactivation in MEFs (37). Finally, our RNA-Seq analysis provided in Fig. 7 of this manuscript clearly showed that additional DNA damage repair genes are down-regulated upon Plk1 overexpression. Thus, Plk1-KI-associated increased cancer formation upon IR is likely due to multiple factors.

Materials and methods

Animal experiments

All procedures involving mice were guided by Purdue University Animal Care and Use Committee (Protocol no. 1111000133E001). Mice housed in the animal facility with free access to standard rodent chow and water were under pathogen-free conditions and maintained in a 12-h light/12-h dark cycle.

Isolation of total RNA from murine tissues

After Plk1-KI and WT mice were quickly killed, different organs were prepared and stored in RNAlater stabilization reagent (Qiagen). For the RNA preparation, tissue pieces of 20 mg were dispersed with a PCR tissue homogenizing kit, followed by total RNA isolation using an RNeasy mini kit (Qiagen).

Establishment of MEFs derived from WT and Plk1-KI embryos

After removing the head and organs of embryos at day 13.5, the tissue was minced and rinsed with PBS, followed by incubation with 0.5 ml of 0.1% trypsin for 20 min at 37 °C. Trypsin was inactivated by addition of 5 ml of DMEM supplemented with 10% FBS. After centrifugation, the cell pellets were resuspended with DMEM and plated onto a 10-cm dish. Medium was changed to remove the large clumps after 24 h. For Plk1-KI MEFs, 5×10^6 cells were treated with 1 mM 4-hydroxytamoxifen for 48 h to induce Plk1 expression. The genotypes of embryos were detected by PCR with primers that are specific to the Plk1 sequence. The cells were cultured at 37 °C with 8% CO_2 in DMEM supplemented with 10% (v/v) fetal calf serum, penicillin, streptomycin, and 50 μM 2-mercaptoethanol. The MEFs were frozen as stocks at the second passage and used for subsequent studies.

Plk1 expression analysis

Real-time RT-PCR was carried out using the primer pairs 5′-TAATGACTCAACACGCCTGATT-3′ and 5′-AGCTCAGCAGCTTGTCTACCAT-3′. The β-actin-specific primers were used as controls: 5′-GAGGAGCACCCCGTGCTGC-3′ and 5′-CCTGCTTGCTGCTGATCCACA-3′. To quantify Plk1 transcripts, 1 μg of RNA was subjected to qRT-PCR. The qRT-PCR was conducted using a TaqMan gene expression assay for murine Plk1. As an internal control in the TaqMan assay, murine β-actin was used (Applied Biosystems). In brief, the 10-μl PCR included 1 μl of RT product, 1 × TaqMan Universal PCR Master Mix, 0.2 μl of TaqMan probe, 1 μl of forward primer, and 1 μl of reverse primer. The reactions were incubated in a 96-well plate at 95 °C (10 min), followed by 40 cycles of 95 °C (15 s) and 60 °C (1 min). All reactions were run in triplicate.

Analysis of mouse genotypes

To test the genotype of WT or Plk1-KI mice, genomic DNA was prepared from tail clips 0.5–0.8 mm in length with Viagen Direct PCR-Tail reagent (Peqlab Biotechnologie, Erlangen, Germany) according to the manufacturer's protocol. For the standard PCR, 10 ng of genomic DNA was amplified using the sense primer 5′-ACTTCGTATAGCATACATTATACGAAGTTATC-3′ and the antisense primer 5′-TCCTTTACCCAGAAAGCGC-3′.

Antibodies

Although the antibodies against ATM (100–104) and phospho-ATM (Ser(P)-1981) (100–81803) were purchased from Novus Biologicals, the antibodies against phospho-Chk2 (Thr(P)-68) (2661), Chk2 (2662) were obtained from Cell Signaling. The antibodies against γ-H2AX (22551) were from Abcam, whereas the antibodies against Plk1 (05-844) were from Millipore.

Immunoblotting

Cell lysates were prepared in TBSN buffer (20 mM Tris-HCl, pH 8.0, 1 mM EDTA, 0.5 mM Na_3VO_4, 5 mM EGTA, 1% Nonidet P-40) supplemented with 150 mM NaCl. For immunoprecipitation, lysates were incubated with antibodies in TBSN at 4 °C overnight, followed by three washes with TBSN plus 500 mM NaCl and three more washes with TBSN plus 150 mM NaCl.

FACS analysis

The cells in culture dishes were trypsinized, washed with PBS, and fixed in 95% ice-cold ethanol overnight. After centrifugation, the cells were resuspended in PBS and incubated with 50 mg/ml propidium iodide in the presence of 100 units/ml RNase A, followed by FACS analysis.

Measurement of energy expenditure

Oxygen consumption (VO_2) and carbon dioxide production (VCO_2) were measured under a consistent environmental temperature and light cycle using an indirect calorimetry system (Oxymax; Columbus Instruments). After the male mice were acclimated to the metabolic chamber for 2 days, VO_2 and VCO_2 were measured in each individual mouse at 15-min intervals during a 48-h period.

Glucose tolerance test

GTT was performed by intraperitoneal injection of D-glucose (Sigma) at a dose of 2 mg/g body weight with an Onetouch Ultra glucometer (Lifescan) into male mice after an overnight fast. Blood glucose levels were then measured at different times (15, 30, 45, 60, 75, and 90 min).

Chromosome aneuploidy

After cells were treated with 50 ng/ml colchicine for 4 h, the cells were collected and hypotonically swollen in 75 nM KCl for 30 min at 37 °C. The cells were fixed in freshly made Carnoys fixative solution (75% methanol, 25% acetic acid) with three changes of fixative. The cells were then dropped onto glass slides and dried at room temperature. Chromosomes were stained with DAPI for 30 m, rinsed with PBS three times, and mounted.

Tumor analysis and histopathology

Aged mice were sacrificed by cervical dislocation following anesthetization with isofluorine. Necropsies were performed, and tissues as well as tumors observed by gross inspection were fixed in 10% formalin 2 days and then embedded in paraffin. For IHC analysis, representative sections were deparaffinized, rehydrated in graded alcohols, and processed using the avidin-biotin immunoperoxidase method. Sections were subjected to antigen retrieval by microwave oven treatment using standard procedures.

RNA-Seq analysis

MEFs were irradiated with 2 Gy γ-ray, incubated for 12 h, and harvested for RNA extraction. Total RNA was extracted from 1×10^7 cells using TRIzol reagent (Life Technologies), followed by purification with the RNeasy mini kit (Qiagen) based on the manufacturer's instructions. Quality of input total RNA was assessed using an Agilent Bioanalyzer RNA nano chip. Libraries were constructed largely as directed by the Illumina TruSeq Stranded mRNA sample preparation guide (catalog no. RS-122-9004DOC), using reagents from the Illumina TruSeq RNA library preparation kit (catalog nos. RS-122-2001 and RS-122-2002). Briefly, poly(A)$^+$ RNA was isolated by annealing biotinylated oligo(dT) to total RNA, followed by capture with streptavidin-conjugated magnetic beads. Non-bound RNAs were then largely removed by discarding the supernatant after magnetic pelleting of Ampure beads. More binding buffer was added followed by an 80 °C incubation to strand denature all RNA from the oligo(dT) captured poly(A)$^+$ RNA, followed by another cycle of binding and supernatant removal. The poly(A)$^+$ RNA was eluted in a divalent cation and hexamer first-strand synthesis primer containing buffer and fragmented with a 4-min incubation at 95 °C. Reverse transcriptase in the presence of actinomycin D to repress any DNA-templated polymerization was used to synthesize first-strand synthesis of cDNA. Second-strand synthesis was performed, replacing dTTP with dUTP, which largely eliminates second-strand amplicons during subsequent amplification. cDNA ends were repaired, 3′-adenylated, and ligated to Illumina adapters. Products were subjected to a 0.8:1 Ampure:sample purification to reduce lower molecular weight amplicons, and the resulting libraries were assessed with an Agilent DNA high sensitivity chip for yield. Based on the overall yields, it was surmised that 8 cycles of amplification, rather than the 15 cycles recommended by the Illumina protocol, would be used. Amplified final libraries were titered for clustering using a KAPA library quantification kit Illumina (KAPA catalog no. KR045), pooled, and clustered in a single HiSeq 2500 v2 Rapid Chemistry lane to generate 60 base single reads. To analyze the data, all sequenced libraries were mapped to the mouse genome (UCSC mm10) using STAR RNA-Seq aligner (37). The uniquely mapped reads were assigned to mm10 refGene genes using featureCounts (from subread) (38). The data were normalized using TMM (trimmed mean of M values) method. The gene expression was finally summarized on base-2 logarithmic scale. We excluded genes with average expression level lower than 1 for all phenotypes. Differential expression analysis was performed using edgeR with paired samples setting (39, 40). The false discovery rate was computed from p values using the Benjamini-Hochberg procedure. Genes with false discovery rates of <0.05 and absolute values of fold change (FC) larger than 1.5 were considered as differentially expressed genes (DEGs).

Statistical analysis

All data are presented as means ± S.D. Statistical calculations were performed with Microsoft Excel analysis tools. Although a two-tailed, unpaired Student's t test was used to assess the difference between the effects of treatment in cell lines, one-way analysis of variance was used to determine statistically significant differences from the means in the animal study. p values of <0.05 were considered statistically significant. *, $p < 0.05$; **, $p < 0.01$.

Author contributions—Z. L. conducted most of the experiments, analyzed the results, and wrote most of the paper. J. Liu, J. Li, Y. K., and G. S. also conducted some of the experiments. X. R., Y. L., and J. W. analyzed RNA-Seq data. X. L. analyzed the data and wrote the paper with Z. L.

Acknowledgments—The RNA-Seq analysis was performed by the Collaborative Core for Cancer Bioinformatics shared by Indiana University Simon Cancer Center and Purdue University Center for Cancer Research with the support from the Walther Cancer Foundation.

References

1. Hanahan, D., and Weinberg, R. A. (2011) Hallmarks of cancer: the next generation. *Cell* **144,** 646–674
2. Hassold, T., Hall, H., and Hunt, P. (2007) The origin of human aneuploidy: where we have been, where we are going. *Hum. Mol. Genet.* **16,** R203–R208

3. Compton, D. A. (2011) Mechanisms of aneuploidy. *Curr. Opin. Cell Biol.* **23,** 109–113
4. Vitale, I., Galluzzi, L., Castedo, M., and Kroemer, G. (2011) Mitotic catastrophe: a mechanism for avoiding genomic instability. *Nat. Rev. Mol. Cell Biol.* **12,** 385–392
5. Vitre, B. D., and Cleveland, D. W. (2012) Centrosomes, chromosome instability (CIN) and aneuploidy. *Curr. Opin. Cell Biol.* **24,** 809–815
6. Lacroix, B., and Maddox, A. S. (2012) Cytokinesis, ploidy and aneuploidy. *J. Pathol.* **226,** 338–351
7. Johnson, L. N. (2011) Substrates of mitotic kinases. *Sci. Signal.* **4,** pe31
8. Sunkel, C. E., and Glover, D. M. (1988) polo, a mitotic mutant of *Drosophila* displaying abnormal spindle poles. *J. Cell Sci.* **89,** 25–38
9. Strebhardt, K. (2010) Multifaceted polo-like kinases: drug targets and antitargets for cancer therapy. *Nat. Rev. Drug Discov.* **9,** 643–660
10. Liu, X. (2015) Targeting polo-like kinases: a promising therapeutic approach for cancer treatment. *Transl. Oncol.* **8,** 185–195
11. Cholewa, B. D., Liu, X., and Ahmad, N. (2013) The role of polo-like kinase 1 in carcinogenesis: cause or consequence? *Cancer Res.* **73,** 6848–6855
12. Gutteridge, R. E., Ndiaye, M. A., Liu, X., and Ahmad, N. (2016) Plk1 inhibitors in cancer therapy: from laboratory to clinics. *Mol. Cancer Ther.* **15,** 1427–1435
13. Liu, X. S., Li, H., Song, B., and Liu, X. (2010) Polo-like kinase 1 phosphorylation of G_2 and S-phase-expressed 1 protein is essential for p53 inactivation during G_2 checkpoint recovery. *EMBO Rep.* **11,** 626–632
14. Yang, X., Li, H., Zhou, Z., Wang, W. H., Deng, A., Andrisani, O., and Liu, X. (2009) Plk1-mediated phosphorylation of Topors regulates p53 stability. *J. Biol. Chem.* **284,** 18588–18592
15. Li, Z., Li, J., Bi, P., Lu, Y., Burcham, G., Elzey, B. D., Ratliff, T., Konieczny, S. F., Ahmad, N., Kuang, S., and Liu, X. (2014) Plk1 phosphorylation of PTEN causes a tumor-promoting metabolic state. *Mol. Cell. Biol.* **34,** 3642–3661
16. Li, Z., Lu, Y., Ahmad, N., Strebhardt, K., and Liu, X. (2015) Low-dose arsenic-mediated metabolic shift is associated with activation of Polo-like kinase 1 (Plk1). *Cell Cycle* **14,** 3030–3039
17. Rödel, F., Keppner, S., Capalbo, G., Bashary, R., Kaufmann, M., Rödel, C., Strebhardt, K., and Spänkuch, B. (2010) Polo-like kinase 1 as predictive marker and therapeutic target for radiotherapy in rectal cancer. *Am. J. Pathol.* **177,** 918–929
18. Hou, X., Li, Z., Huang, W., Li, J., Staiger, C., Kuang, S., Ratliff, T., and Liu, X. (2013) Plk1-dependent microtubule dynamics promotes androgen receptor signaling in prostate cancer. *Prostate* **73,** 1352–1363
19. Shao, C., Ahmad, N., Hodges, K., Kuang, S., Ratliff, T., and Liu, X. (2015) Inhibition of polo-like kinase 1 (Plk1) enhances the antineoplastic activity of metformin in prostate cancer. *J. Biol. Chem.* **290,** 2024–2033
20. Li, J., Wang, R., Schweickert, P. G., Karki, A., Yang, Y., Kong, Y., Ahmad, N., Konieczny, S. F., and Liu, X. (2016) Plk1 inhibition enhances the efficacy of gemcitabine in human pancreatic cancer. *Cell Cycle* **15,** 711–719
21. Song, B., Liu, X. S., Rice, S. J., Kuang, S., Elzey, B. D., Konieczny, S. F., Ratliff, T. L., Hazbun, T., Chiorean, E. G., and Liu, X. (2013) Plk1 phosphorylation of orc2 and hbo1 contributes to gemcitabine resistance in pancreatic cancer. *Mol. Cancer Ther.* **12,** 58–68
22. Zhang, Z., Hou, X., Shao, C., Li, J., Cheng, J. X., Kuang, S., Ahmad, N., Ratliff, T., and Liu, X. (2014) Plk1 inhibition enhances the efficacy of androgen signaling blockade in castration-resistant prostate cancer. *Cancer Res.* **74,** 6635–6647
23. Strebhardt, K., Becker, S., and Matthess, Y. (2015) Thoughts on the current assessment of Polo-like kinase inhibitor drug discovery. *Expert Opin. Drug. Discov.* **10,** 1–8
24. Lee, K. S., Burke, T. R., Jr., Park, J. E., Bang, J. K., and Lee, E. (2015) Recent advances and new strategies in targeting Plk1 for anticancer therapy. *Trends Pharmacol. Sci.* **36,** 858–877
25. Schwenk, F., Baron, U., and Rajewsky, K. (1995) A cre-transgenic mouse strain for the ubiquitous deletion of loxP-flanked gene segments including deletion in germ cells. *Nucleic Acids Res.* **23,** 5080–5081
26. van Vugt, M. A., Brás, A., and Medema, R. H. (2004) Polo-like kinase-1 controls recovery from a G_2 DNA damage-induced arrest in mammalian cells. *Mol. Cell* **15,** 799–811
27. Bensimon, A., Aebersold, R., and Shiloh, Y. (2011) Beyond ATM: the protein kinase landscape of the DNA damage response. *FEBS Lett.* **585,** 1625–1639
28. Malumbres, M., and Barbacid, M. (2007) Cell cycle kinases in cancer. *Curr. Opin. Genet. Dev.* **17,** 60–65
29. Scharow, A., Knappe, D., Reindl, W., Hoffmann, R., and Berg, T. (2016) Development of bifunctional inhibitors of polo-like kinase 1 with low-nanomolar activities against the polo-box domain. *ChemBioChem* **17,** 759–767
30. Baudino, T. A., Maclean, K. H., Brennan, J., Parganas, E., Yang, C., Aslanian, A., Lees, J. A., Sherr, C. J., Roussel, M. F., and Cleveland, J. L. (2003) Myc-mediated proliferation and lymphomagenesis, but not apoptosis, are compromised by E2f1 loss. *Mol. Cell* **11,** 905–914
31. Wagner, A. J., Kokontis, J. M., and Hay, N. (1994) Myc-mediated apoptosis requires wild-type p53 in a manner independent of cell cycle arrest and the ability of p53 to induce p21waf1/cip1. *Genes Dev.* **8,** 2817–2830
32. Zhang, D., Hirota, T., Marumoto, T., Shimizu, M., Kunitoku, N., Sasayama, T., Arima, Y., Feng, L., Suzuki, M., Takeya, M., and Saya, H. (2004) Cre-loxP-controlled periodic Aurora-A overexpression induces mitotic abnormalities and hyperplasia in mammary glands of mouse models. *Oncogene* **23,** 8720–8730
33. Raab, M., Kappel, S., Krämer, A., Sanhaji, M., Matthess, Y., Kurunci-Csacsko, E., Calzada-Wack, J., Rathkolb, B., Rozman, J., Adler, T., Busch, D. H., Esposito, I., Fuchs, H., Gailus-Durner, V., Klingenspor, M., *et al.* (2011) Toxicity modelling of Plk1-targeted therapies in genetically engineered mice and cultured primary mammalian cells. *Nat. Commun.* **2,** 395
34. Hyun, S. Y., Hwang, H. I., and Jang, Y. J. (2014) Polo-like kinase-1 in DNA damage response. *BMB Rep.* **47,** 249–255
35. Li, Z., Li, J., Kong, Y., Yan, S., Ahmad, N., and Liu, X. (2017) Plk1 phosphorylation of Mre11 antagonizes the DNA damage response. *Cancer Res.* **77,** 3169–3180
36. Liu, X., and Erikson, R. L. (2003) Polo-like kinase (Plk)1 depletion induces apoptosis in cancer cells. *Proc. Natl. Acad. Sci. U.S.A.* **100,** 5789–5794
37. Dobin, A., Davis, C. A., Schlesinger, F., Drenkow, J., Zaleski, C., Jha, S., Batut, P., Chaisson, M., and Gingeras, T. R. (2013) STAR: ultrafast universal RNA-Seq aligner. *Bioinformatics* **29,** 15–21
38. Liao, Y., Smyth, G. K., and Shi, W. (2014) featureCounts: an efficient general purpose program for assigning sequence reads to genomic features. *Bioinformatics* **30,** 923–930
39. Robinson, M. D., McCarthy, D. J., and Smyth, G. K. (2010) edgeR: a Bioconductor package for differential expression analysis of digital gene expression data. *Bioinformatics* **26,** 139–140
40. McCarthy, D. J., Chen, Y., and Smyth, G. K. (2012) Differential expression analysis of multifactor RNA-Seq experiments with respect to biological variation. *Nucleic Acids Res.* **40,** 4288–4297